Chemical Engineering Journal 382 (2020) 122883

Contents lists available at ScienceDirect

Chemical Engineering Journal

journal homepage: www.elsevier.com/locate/cej

High-gravity-assisted preparation of aqueous dispersions of monodisperse palladium nanocrystals as pseudohomogeneous catalyst for highly efficient nitrobenzene reduction

Jin-Tao Du[a,b], Jie Shi[b], Qian Sun[a,b], Dan Wang[a,b,*], Hao Wu[b], Jie-Xin Wang[a,b,*], Jian-Feng Chen[a,b]

[a] Beijing Advanced Innovation Center for Soft Matter Science and Engineering, State Key Laboratory of Organic-Inorganic Composites, Beijing University of Chemical Technology, Beijing 100029, PR China
[b] Research Center of the Ministry of Education for High Gravity Engineering and Technology, Beijing University of Chemical Technology, Beijing 100029, PR China

HIGHLIGHTS

- Size-tunable monodisperse Pd nanocrystals were prepared in a rotating packed bed.
- They were adopted as pseudohomogeneous catalyst for nitrobenzene (NB) reduction.
- 2.6 nm Pd nanocrystals displayed excellent catalytic property and good stability.
- The obtained catalytic kinetics data confirm to the Langmuir-Hinshelwood model well.
- DFT calculation was used to study the adsorption of NB on the surface of catalyst.

GRAPHICAL ABSTRACT

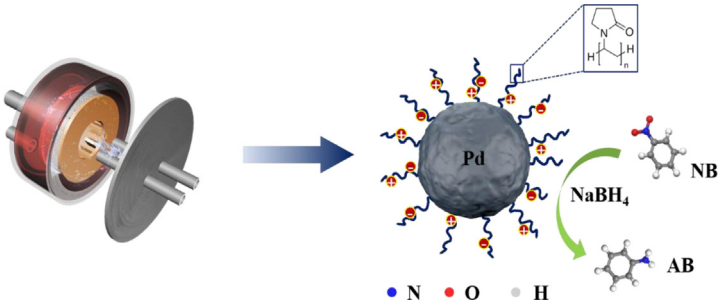

ARTICLE INFO

Keywords:
Pseudohomogeneous catalyst
Monodispersed palladium nanocrystals
High gravity
Nitrobenzene reduction
Density functional calculation

ABSTRACT

Nitrobenzene (NB) reduction is an important catalytic reaction, which is commonly performed in aqueous medium mainly with heterogeneous catalysts. In this work, highly stable aqueous nanodispersions of Pd nanocrystals with a tunable average size between 2 and 11 nm are conveniently prepared in a high-gravity rotating packed bed (RPB) reactor, and firstly serve as a pseudohomogeneous catalyst for NB reduction. As compared to a conventional stirred tank reactor (STR), the product prepared in the RPB reactor has a more uniform particle size. More importantly, the reaction time can be greatly shortened from 3 min (STR) to 1 s (RPB), thereby realizing a continuous preparation. This Pd pseudohomogeneous catalyst displays a significantly size-dependent catalytic activity and a good stability performance. Ultra-small 2.6 nm Pd nanocrystals have a reaction rate five times as fast as 10.1 nm counterpart. The obtained kinetics data confirm to the Langmuir-Hinshelwood model well, having a small error of < 10%. Furthermore, the adsorption behavior of NB molecules on the surface of Pd nanocrystals was also studied with density functional theory (DFT) calculation. Since the processing capacity of the used lab-scale RPB reached 44.2 g/h, this route may offer a general platform for mass production of monodisperse nanocrystals as pseudohomogeneous catalyst for highly efficient catalysis.

* Corresponding authors at: Beijing Advanced Innovation Center for Soft Matter Science and Engineering, State Key Laboratory of Organic-Inorganic Composites, Beijing University of Chemical Technology, Beijing 100029, PR China.
E-mail addresses: wangdan@mail.buct.edu.cn (D. Wang), wangjx@mail.buct.edu.cn (J.-X. Wang).

https://doi.org/10.1016/j.cej.2019.122883
Received 4 July 2019; Received in revised form 9 September 2019; Accepted 18 September 2019
Available online 19 September 2019
1385-8947/

1. Introduction

Upon wide application of nitrobenzene (NB), a set of related environmental issues containing the contamination of soil and water resources have been put forward due to its stability and toxicity, which was even established as a carcinogen in the list of Class 2B [1]. Hence, it is important to convert NB into less toxic compounds, thereby eliminating the toxic substance and synthesizing high-value chemicals such as aniline (AB) [2–6], which is an indispensable intermediate in the synthesis of organic pigments, pesticides, explosives, and polymers [7–12].

The reduction of NB to AB is commonly performed in aqueous medium mainly using metal-based heterogeneous catalysts, such as those containing Ag, Pt Pd, Fe and Au [13–17]. Among them, Pd-based catalyst has gained the most attention owing to its excellent catalytic performances [18–20]. However, there are still several challenges in the application of these heterogeneous catalysts for NB reduction. Firstly, it is desired for catalysts to be well dispersed in an aqueous medium, allowing enhanced complete contact between NB molecules and catalysts, which is difficult for heterogeneous catalysts to achieve. Secondly, the diffusion between the carrier and supported catalytic centers leads to their relatively low utilization and activity. To resolve these problems, it is helpful and feasible to design and develop novel pseudohomogeneous catalysts, which can be uniformly dispersed in solvent [21–23]. If active component such as Pd is made into ultrasmall Pd nanocrystals with good dispersity and stability in water, pseudohomogeneous catalysis can be well achieved, thereby completely exhibiting its excellent catalytic activity.

Rotating packed bed (RPB) is a novel process intensification apparatus, which can create high gravity environment with a homogeneous spatial distribution of concentration, temperature, and supersaturation. This is beneficial to the homogeneous nucleation and growth of particles. Thus, it has been demonstrated as an efficient tool to prepare nanoparticles in a simple, fast and good-handling way [24]. Numerous metals, inorganic and organic nanoparticles have been synthesized by using RPB reactors [25–28]. However, to our best knowledge, there is no report on the preparation of palladium nanocrystals in RPB.

Herein, we present a high-gravity strategy to conveniently prepare highly stable aqueous dispersions of monodispersed Pd nanocrystals with tunable sizes of 2–11 nm and narrow PSD, which is firstly adopted as pseudohomogeneous catalyst for NB reduction. The effects of the nanocrystal size, concentrations of catalyst, NB and reducing agent were explored. Furthermore, the reaction kinetics were investigated. And density functional theory (DFT) calculation was also carried out to better understand the adsorption behavior of NB molecules on the surface of Pd nanocrystals in the catalytic reaction.

2. Experimental section

2.1. Chemicals

Sodium tetrachloropalladate (Na_2PdCl_4) and L-ascorbic acid (AA) were purchased from Shanghai Aladdin Bio-Chem Technology Co. Poly (vinyl pyrrolidone) (PVP, MW: 8000), acetone and ethanol were provided by Beijing Chemical Reagent Co. Nitrobenzene was obtained from Shanghai Macklin Biochemical Technology Co. The chemical reactants were all analytically pure and used as received. Deionized water was prepared by a water purification system (RO-DI plus, Hitech, PRC) and used in all experiments.

2.2. Preparation of aqueous dispersions of monodispersed Pd nanocrystals with tunable sizes

For this reaction system, high temperature can obviously accelerate the nucleation and reaction rates, thereby obtaining the smaller Pd nanocrystals. There are two kinds of RPB reactors with different structures in this study. One is the commonly-used typical RPB reactor with an ultrashort residence time (< 1 s), which is suitable for those fast reaction or precipitation processes. The other is the internal circulation rotating packed bed (ICRPB), which can continuously provide a high-gravity environment for the nucleation and growth of nanoparticles during the relatively slow reaction process [29].

In a typical preparation process with a high reaction temperature of 90 °C, 1575 mg PVP and 5 mmol of AA were added to 240 mL of deionized water. The resultant solution was stored in tank A. 90 mL of the Na_2PdCl_4 aqueous solution with a concentration of 0.032 mol/L was prepared in tank B. The liquid streams from tank A and tank B were pumped with respective flow rates of 533 and 200 mL/min into the typical RPB at a rotating speed of 1500 rpm, and then sprayed through slotted pipe distributor in the reactor. Afterwards, the mixture flowed in the radial direction by the force of centrifugation, passed the porous packing layer and left the reactor through the liquid outlet for collection. Finally, the product was washed with the mixed solution of acetone and ethanol, collected by centrifugation, and then dispersed in water to form an aqueous dispersion of Pd nanocrystals with an average size of 2.6 nm.

For the preparation process with a lower reaction temperature of 60, 45 and 30 °C, the mixed reactant stored in tank A was firstly poured into the ICRPB with a temperature-controlled jacket. Further, the Na_2PdCl_4 solution from tank B was rapidly added into the ICRPB at the same rotating speed of 1500 rpm. The mixture was transported by the liquid lifter to the center of the rotor, flowed radially under centrifugal force, passed the packing, and went back to the bottom cavity of the device under gravity. The whole process was circulated repeatedly. After 10 min, the product was treated with the same above process, thereby achieving the aqueous dispersions of Pd nanocrystals with different average sizes of 4.7, 5.6 and 10.1 nm.

2.3. Catalytic nitrobenzene reduction

The reduction of NB was performed without magnetic stirring. In a typical procedure, 3 mL of an aqueous solution consisting of 1.44 μmol NB and 198 μmol $NaBH_4$ was syringed into a quartz cuvette (4.5 cm × 1.25 cm × 1.25 cm) along with 15 μL of aqueous dispersion of Pd nanocrystals (10 ppm). The absorbance spectrum of the sample in cuvette was scanned on a UV–Vis spectrophotometer in a scanning range of 215–380 nm at room temperature. In the catalytic reduction of NB, the different concentrations of catalyst, NB and $NaBH_4$ were studied. According to the Beer-Lambert law, the absorbance intensity of a solution is proportional to its concentration in a certain region, therefore the changes in absorption intensity directly mean the reduction process. In this reaction, the peak intensities of absorbance were noted at 267 nm to calibrate the concentrations of NB. The catalytic performance of Pd nanocrystals with different sizes were investigated for comparison. Furthermore, the stability measurement was performed. 0.15 mL of an aqueous solution consisting of 1.44 μmol NB was further added after the reaction was completed. This procedure was repeated four times.

2.4. DFT calculation

First-principle calculations based on spin polarized DFT were performed using the Vienna ab initio simulation package (VASP.5.4.1) [30]. The reparameterized Perdew–Burke–Ernzerhof (revPBE) form of the generalized gradient approximation (GGA) was used to calculate nonlocal gradient corrections to the correlation and exchange energies [31,32]. The wave functions were constructed from the expansion of plane waves with an energy cutoff of 450 eV. The electron ion interactions in the core region were described by Vanderbilt ultrasoft pseudopotentials with real space projection operators [33]. A 2 × 2 × 1 Monkhorst-Pack k-point sampling in the surface Brillouin zone was performed for the surfaces, and a vacuum layer of 16 Å was

set to avoid interactions between the periodic slabs. For accuracy, the density of states (DOS) was calculated at the k-point of 5 × 5 × 1. Geometric optimization was performed using a 4-layer adsorption model of 144 Pd atoms, with the bottom two layers being fixed. Structural optimizations were carried out at a tight convergence of 0.01 eV/Å on the forces with the wave functions converged to 1×10^{-5} eV. In order to accurately describe the dispersion interactions between the adsorbate and the surface, all calculations were performed using the Rutgers-Chalmers van der Waals Density Functional (vdw-DF) method [34].

2.5. Characterization

The size, morphology, and lattice structure of Pd nanocrystals were examined using a transmission electron microscope (TEM) (H-9500, HITACHI, Japan) operating at an accelerating voltage of 300 KV. The crystalline structure of Pd nanocrystals was exhibited by X-ray diffraction (XRD) (Bruker, Germany) equipped with CuKa radiation source and working at 40 kV and 40 mA. The diffractograms were acquired in the 2θ range from 30° to 90° with a scanning rate of 5°/min and a step size of 0.02°. Surface composition was performed by X-ray photoelectron spectroscopy (XPS) (AXIS Supra, Shimadzu, Japan) with an Al Ka X-ray excitation (600 w). Binding energy (BE) calibration was carried out with amorphous C 1s signal located at 284.6 eV. Elemental analyses were quantified by inductively coupled plasma atomic emission spectroscopy (ICP-AES) (ICPS-7500, Shimadzu, Japan). The optical spectra of the sample were recorded in the range of 215–380 nm using UV–Vis spectrophotometer (UV-2600, Shimadzu, Japan).

3. Results and discussion

Fig. 1 shows the representative TEM images, HRTEM images, selected area electron diffraction (SAED) images and the corresponding particle size distributions of the aqueous dispersions of Pd nanocrystals with different sizes prepared at different temperatures. It can be obviously seen that the Pd nanocrystals are monodispersed and appear sphere-like shape with no specific other shapes. The average diameter of Pd nanocrystals becomes dramatically decreased from 10.1 to 2.6 nm, and the size distribution is narrower with increasing the temperature from 30 to 90 °C. This is possibly because higher temperature results in the faster rate of nucleation [35–37]. When the amount of the precursor is equal, the size of the final products and the number of seeds will be inversely proportional to each other. Moreover, the lattice images of isolated Pd nanocrystals clearly show that the high crystallinity of the as-prepared crystals and the spacing of 0.22 nm corresponded to (1 1 1) planes of Pd structure. SAED images of 10.1 nm Pd nanocrystals show four Debye-Scherrer rings indexed as (1 0 0), (2 0 0), (2 2 0) and (3 1 1) planes of a fcc lattice. In this preparation process, PVP acts as a capping agent, thereby preventing the aggregation and growth of Pd nanocrystals. Furthermore, the aqueous dispersions of Pd nanocrystals can maintain a long-term stability for over 6 months with little precipitation.

For comparison, the aqueous dispersion of Pd nanocrystals was also synthesized in a conventional stirred tank reactor (STR) at 90 °C. Fig. 2 exhibits the TEM images of Pd nanocrystals synthesized at different reaction times in the STR. With the prolonged reaction time, Pd nanocrystals have a gradual improvement of the adhesion phenomenon among particles, and a good dispersity after 3 min. This can be ascribed to this fact that the incomplete micromixing state in the STR greatly affects the nucleation of Pd nanocrystals and the adsorption of PVP molecules on the surfaces of Pd nanocrystals. With the extension of time, PVP molecules are further adsorbed on Pd nanocrystals, thereby achieving enough space resistance to form well-dispersed nanoparticles. By comparison, it can be clearly seen that the product in the RPB reactor has a more uniform particle size than that in the STR. More importantly, the required reaction time is greatly shortened from 3 min

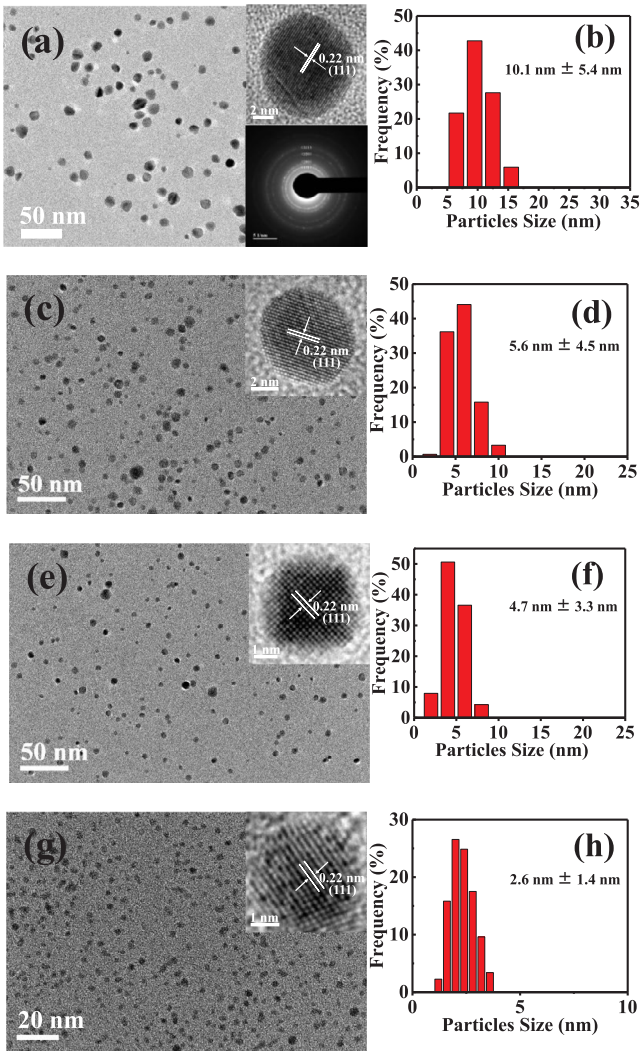

Fig. 1. TEM images and corresponding particle size distributions of Pd nanocrystals synthesized using RPB at 30 °C (a, b), 45 °C (c, d), 60 °C (e, f) and 90 °C (g, h). The insets display the corresponding HRTEM and SAED images of individual nanoparticles.

(STR) to 1 s (RPB). This can be attributed to the significant intensification of micromixing and mass transfer in RPB, favoring the fast and uniform adsorption of PVP. Scheme 1 presents the schematic diagram of the preparation processes of Pd nanocrystals in RPB and STR. Since the processing capacity of this lab-scale RPB reactor with a continuous operation can reach 44.2 g/h, this preparation process is a feasible strategy for mass production of monodisperse Pd nanocrystals.

Fig. 3 shows the XRD patterns of the as-prepared Pd nanocrystals with different sizes. The typical diffraction peaks at around 40°, 46°, 68°, 82° and 86° correspond to the (1 1 1), (2 0 0), (2 2 0), (3 1 1) and (2 2 2) planes of the cubic phase of Pd, respectively. This indicates that Pd nanocrystals have fcc structures, which is in a good agreement with the above SAED data. Moreover, the diffraction peaks become considerably broadened with an increase in the reaction temperature, implying a decrease in Pd nanocrystal size. In particular, for the 2.6 nm Pd nanocrystals, only a broad (1 1 1) peak is obviously discernible, as shown in curve d. This may be caused by the very small size of the nanocrystals [38,39]. Furthermore, the diffraction peaks shift to lower values as the nanocrystal size decreases, proving that the interatomic distance of Pd-Pd has been expanded [40].

Fig. 4 depicts the X-ray photoelectron spectroscopy (XPS) spectra of Pd 3d regions of Pd nanocrystals with different sizes. There are two

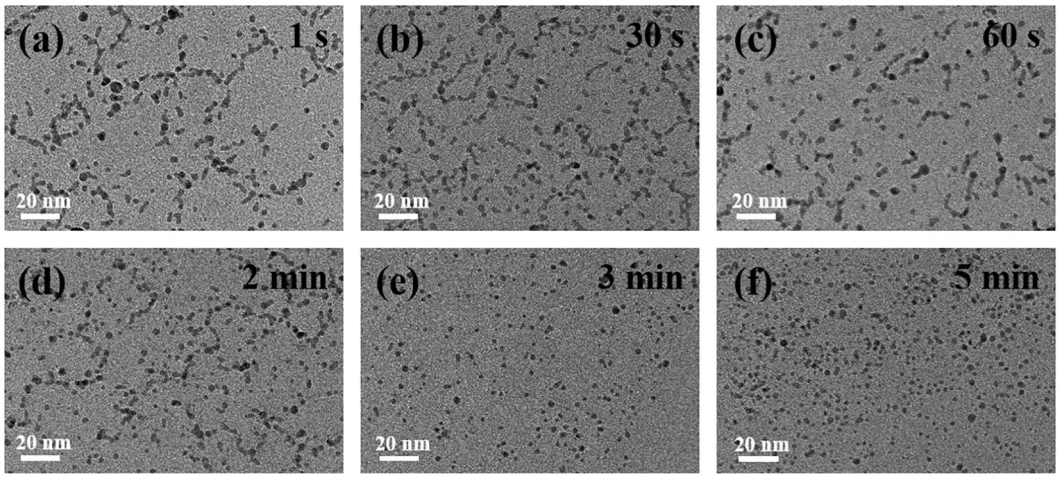

Fig. 2. TEM images of Pd nanocrystals synthesized at different reaction times in the STR: (a) 1 s, (b) 30 s, (c) 60 s, (e) 2 min, (f) 3 min and (g) 5 min.

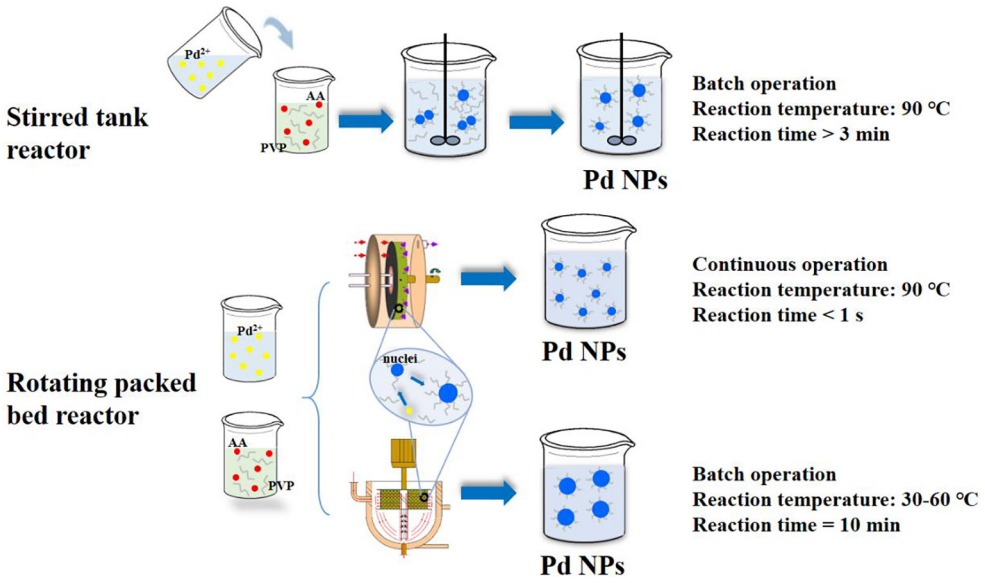

Scheme 1. Schematic diagram of the preparation processes of Pd nanocrystals in RPB and STR.

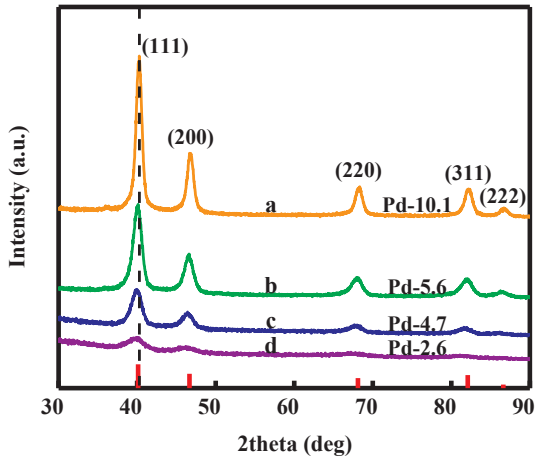

Fig. 3. XRD patterns of Pd nanocrystals with different sizes prepared at different reaction temperatures.

main peaks with binding energies at 340.3–340.7 and 335.1–335.2 eV, corresponding to Pd $3d_{3/2}$ and Pd $3d_{5/2}$, respectively, which means the formation of metallic Pd. In addition, two shoulders were observed for Pd 3d regions with binding energies at 336.3–337 eV, assigned to oxidized Pd species. It can be clearly seen that with the decreasing of particle sizes, the ratio of oxidized Pd was significantly increased, compared with the reduced Pd. This is because Pd nanocrystals with smaller sizes are more susceptible to oxidation [41].

Fig. 5 presents the successive UV–Vis spectra of the catalytic reduction of NB monitored at different times. The intensity of the NB absorbance peak at 267 nm has a rapid decline with the reaction time. Simultaneously, there is an increased intensity of the absorption peak at 232 nm belonging to aniline (AB), indicating the generation of AB from the NB reduction. The λ_{max} of NB has a gradual red shift to 280 nm as catalytic reaction continued. The isosbestic point at 243 nm indicates the formation of no by-products in the whole reaction process [42]. Since the initial concentration of $NaBH_4$ used for the reduction is > 100 times higher than the concentration of NB, it could be considered to be constant. Accordingly, the reduction rate is only related with the concentration of NB, conforming to the pseudo first order kinetics. The apparent kinetic rate constant (k_{app}) is calculated from the following equation.

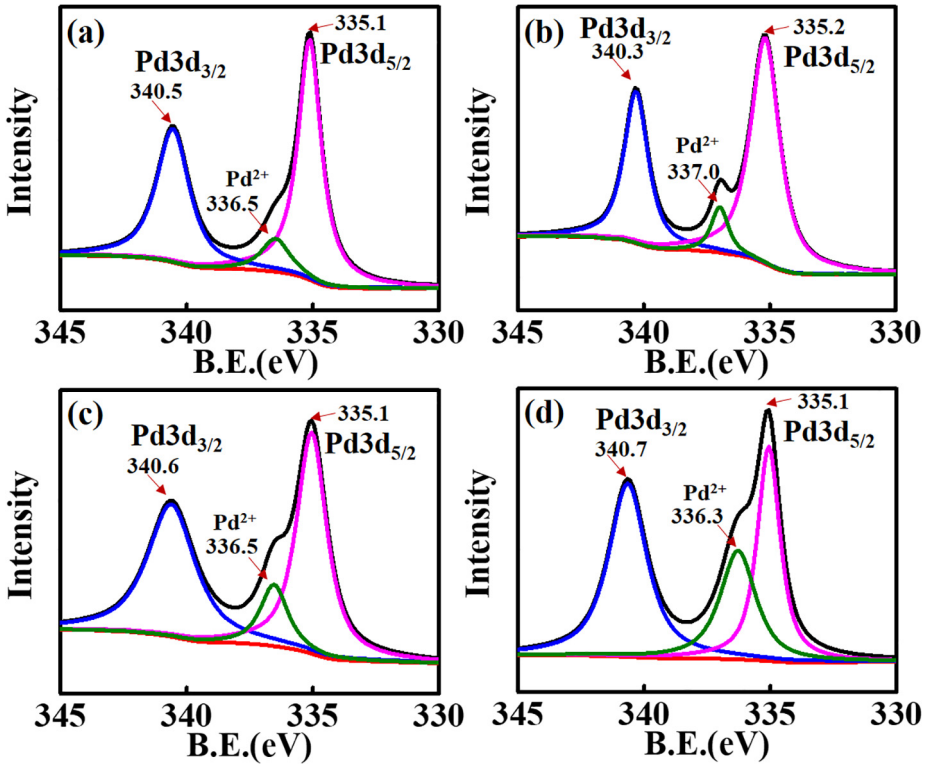

Fig. 4. XPS images of Pd nanocrystals using RPB at 30 °C (a), 45 °C (b), 60 °C (c) and 90 °C (d).

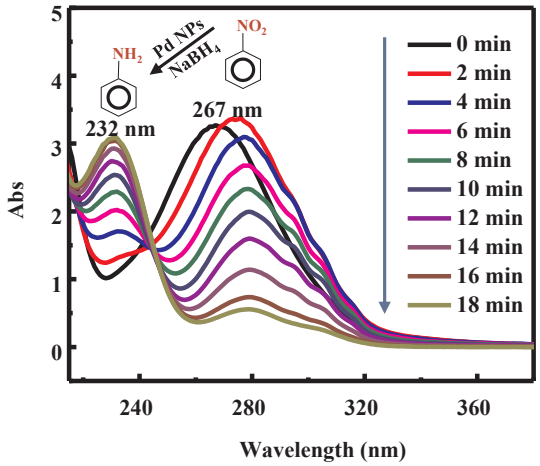

Fig. 5. UV–Vis spectra of the reduction of NB catalyzed by Pd nanocrystals (reaction conditions: C_{NB}: C_{NaBH_4} = 1:137, room temperature, C_{Pd} = 0.45 μmol/L, size:5.6 nm).

$$\ln\frac{A_t}{A_0} = \ln\frac{C_t}{C_0} = k_{app} \times t \quad (1)$$

where A_0 and A_t are the NB absorbance values at 267 nm at the beginning and t time, respectively. C_0 and C_t are the NB concentrations corresponding to absorbance A_0 and A_t, respectively.

Fig. 6 shows the curves of $\ln(A_t/A_0)$ versus reaction time, and TEM image of 2.6 nm Pd nanocrystals after catalytic reaction. As shown in Fig. 6(a), there is nearly no change in the value of $\ln(A_t/A_0)$ without Pd catalyst, indicating little NB is reduced. However, the value of $\ln(A_t/A_0)$ almost linearly and rapidly declines, and becomes stationary as Pd nanocrystals are introduced to this reaction system. And the smaller Pd nanocrystals result in the faster decrease of the value of $\ln(A_t/A_0)$, demonstrating the significant enhancement of NB reduction rate. Thus, the apparent rate constant k_{app} can be obtained from the linear slope. The results indicate that the catalytic activity (k_{app}) of 2.6 nm Pd nanocrystals is ca. 5 and 2 times higher than those of 10.1 nm nanocrystals and 5.6 nm nanocrystals, respectively. Furthermore, 2.6 nm Pd nanocrystals still keep monodispersed and appear sphere-like shape with nearly unchanged size after catalytic reaction, as shown in Fig. 6(b).

In this catalytic reduction process, the reaction rate is affected by a two-step mechanism: (a) adsorption of NB and $NaBH_4$ onto the catalyst surface; and (b) interfacial electron transfer and detachment of AB away from the surface, which helps overcoming the kinetic barrier of electron transfer from $NaBH_4$ to NB. Therefore, the reaction conditions, including the surface area of catalyst, the initial concentrations of NB and $NaBH_4$, have important effects on the value of k_{app}. Fig. 7 presents the dependence of k_{app} on the concentrations of Pd nanocrystals, NB and $NaBH_4$ as well as catalytic stability property. Fig. 7(a) shows the plot of k_{app} as a function of catalyst dosages and sizes. The values of k_{app} linearly will increase with increasing the usage amount of Pd nanocrystals. Additionally, the slopes of the straight lines increase with decreasing the Pd nanocrystal sizes. Increasing the catalyst dosage and decreasing the catalyst size will lead to a faster reduction rate of nitrobenzene due to the increased number of the active sites and a faster electron transfer. Fig. 7(b) and (c) display the dependence of k_{app} on C_{NB} and C_{NaBH_4}, respectively. k_{app} is markedly decreased with an increasing concentration of NB. For a constant concentration of NB, k_{app} is first increased and then leveled off (10.1 and 5.6 nm) or decreased (2.6 nm) with increasing the concentration of $NaBH_4$. Moreover, Pd nanocrystals with smaller size are more sensitive to the variation of the initial concentration of reactants. This characteristic dependence of k_{app} corresponds to Langmuir-Hinshelwood model. Both reactants compete for free active sites at the surface of the Pd nanoparticles, and the reaction can occur only between species adsorbed on the surface [17]. The reduction will be slowed down considerably if most active sites are occupied by a single reactant. Number of active sites increases with the decrease in particle size, thereby exhibiting a high performance and changing the sensitivity to the concentration of reactants. In Fig. 7(d),

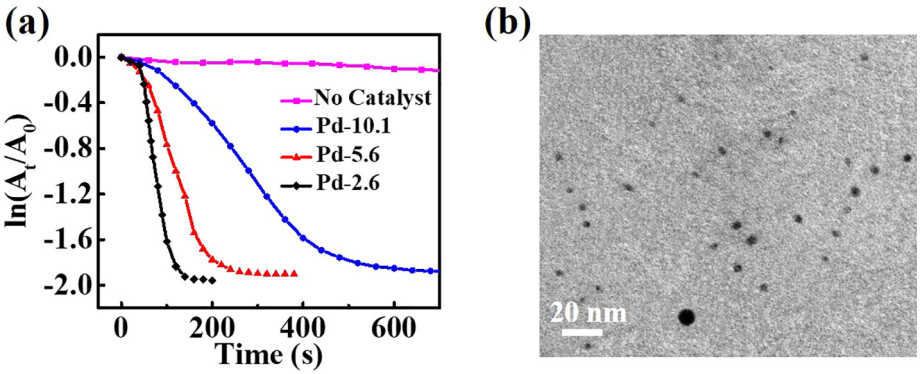

Fig. 6. (a) Curves of $\ln(A_t/A_0)$ versus reaction time (reaction conditions: C_{NB}: C_{NaBH_4} = 1:137, room temperature, C_{Pd} = 1.5 μmol/L). (b) TEM image of 2.6 nm Pd nanocrystals after catalytic reaction.

the stability of 2.6 nm Pd nanocrystals was investigated by adding the fresh NB aqueous solution. The k_{app} of five cycles was 0.025, 0.024, 0.022 0.020 and 0.018 s^{-1} in turn. The catalytic activity of Pd nanocrystals is slightly decreased within five experiments because of the consumption of $NaBH_4$ and the dilution of catalysts.

The Langmuir-Hinshelwood (L-H) model is used to fit above experimental results [43].

$$\frac{dC_{NB}}{dt} = -k_{app} \cdot C_{NB} = -k \cdot S \cdot \theta_{NB} \cdot \theta_{BH_4^-} \quad (2)$$

where k represents the intrinsic rate constant; S is the total surface of all Pd nanocrystals; and θ_{NB} and $\theta_{BH_4^-}$ denote the surface coverages of NB and BH_4^- on Pd nanocrystals, respectively, which can be modeled in terms of the Langmuir-Freundlich isotherm.

$$\theta_i = \frac{(K_i C_i)^{n_i}}{1 + \sum_{j=1}^{N} (K_j C_j)^{n_j}} \quad (3)$$

where K_i denotes the adsorption constant of the respective component and C_i is the concentration. The exponent n is related to the heterogeneity of the surface. With these definitions, Eq. (2) can be rewritten as [17,44].

$$k_{app} = \frac{k \cdot S \cdot K_{NB}^{n} \cdot C_{NB}^{n-1} \cdot K_{BH_4^-}^{m} \cdot C_{BH_4^-}^{m}}{(1 + (K_{NB} \cdot C_{NB})^{n} + (K_{BH_4^-} \cdot C_{BH_4^-})^{m})^2} \quad (4)$$

Table 1
k·S, K_{NB} and K_{NaBH_4} from fitting the experimental data to the L-H model shown in Fig. 8.

	k·S (mmol/min)	K_{NB} (L/mmol)	K_{NaBH_4} (L/mmol)	n	m
Pd-10.1 nm	0.2	6.32	0.04	1	0.6
Pd-5.6 nm	0.4	4.38	0.03	1	0.6
Pd-2.6 nm	4	0.70	0.01	0.9	1.3

The parameters in the model were summarized in Table 1. Corresponding to the Pd nanocrystals with three sizes, the L-H expressions are derived as follows

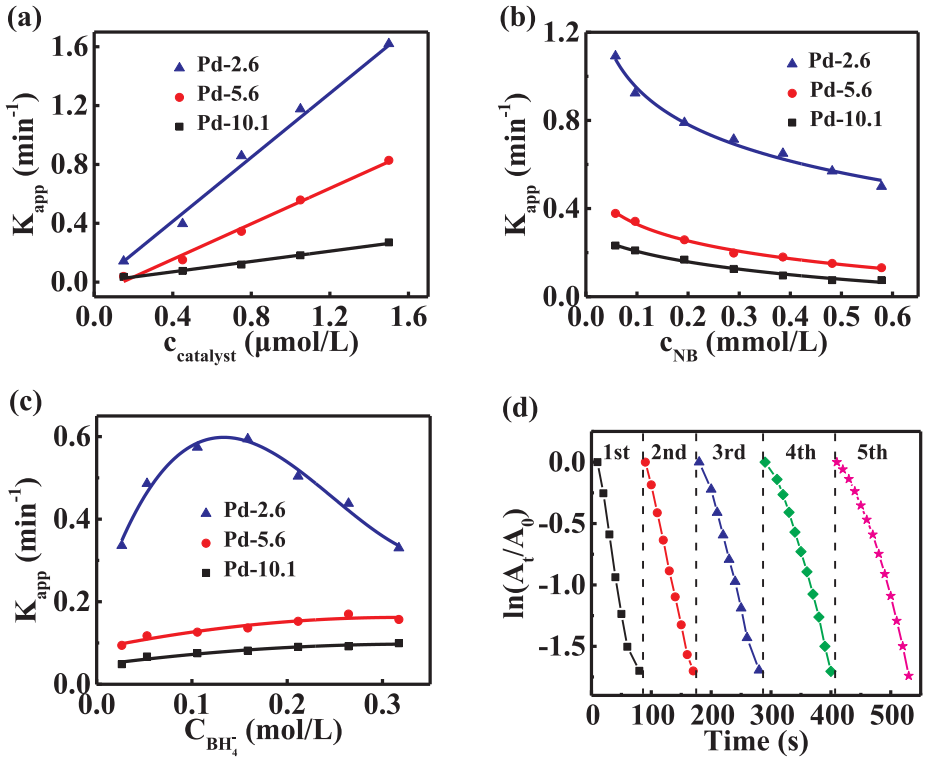

Fig. 7. Plots of k_{app} as a function of (a) catalyst dosage, (b) C_{NB}, (c) C_{NaBH_4}. (d) Stability of Pd nanocrystals.

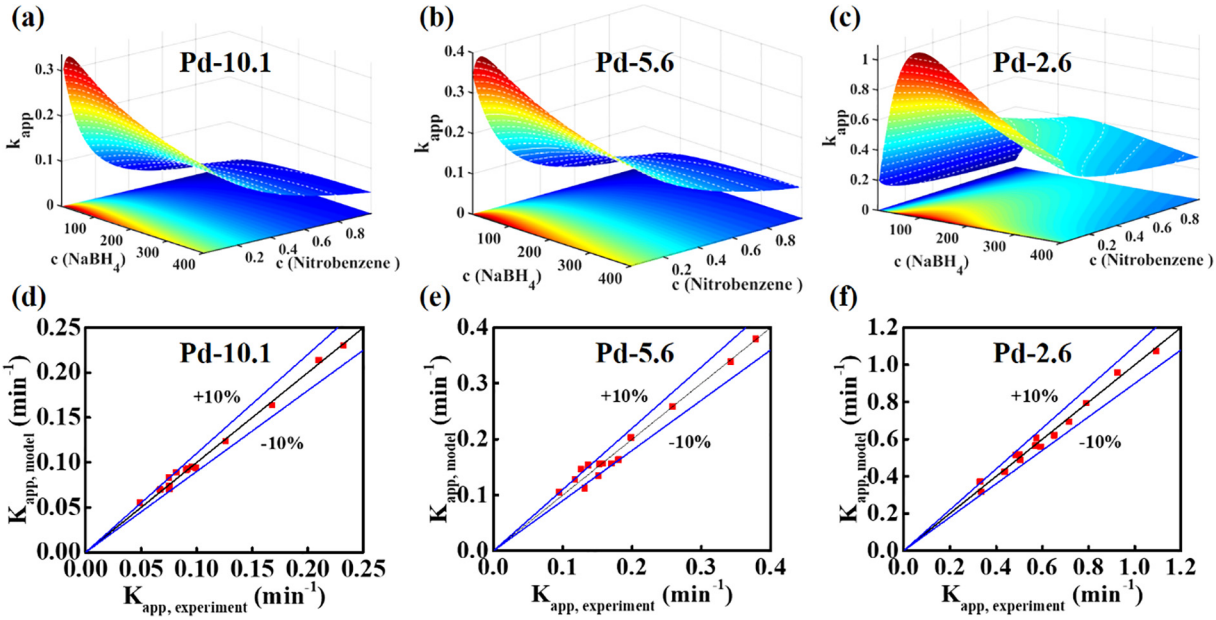

Fig. 8. (a–c) 3D plots of k_{app} as a function of C_{NB} and $C_{BH_4^-}$. (d–f) Comparison of the experimental and theoretical (L-H equation) k_{app} values.

Table 2
Comparison of reported catalysts for the reduction of NB.

C_{NB}/μmol/L	Reducing agent	Temperature/K	Time/h	Catalyst	C_{center}[a]/μmol/L	Activity[b]/h^{-1}	Reference
489	$NaBH_4$	RT	0.0333	Pd-2.6	1.54	8009	This work
489	$NaBH_4$	RT	0.0556	Pd-5.6	1.54	4746	This work
489	$NaBH_4$	RT	0.1667	Pd-10.1	1.54	1606	This work
200,000	$NaBH_4$	RT	6	Pd-polymer	3500	9	[15]
50,000	$NaBH_4$	RT	3	Pd-rGO	176	95	[45]
500,000	$NH_2NH_2{\cdot}H_2O$	353	2.5	Pd-CSs	250	800	[46]
200,000	Formic acid	333	7	Pd/NH_2-UiO-66	658	43	[47]
100,000	$NH_3{\cdot}BH_3$	RT	0.0833	Ag/Pd-rGO	196	6079	[48]
100,000	$NaBH_4$	RT	2	Ni-polymer	1860	24	[49]
100,000	$NH_3{\cdot}BH_3$	RT	0.25	Fe_{48}/Pd_{52}-rGO	923	429	[50]
100,000	$NH_3{\cdot}BH_3$	RT	0.0833	$Ni_{30}Pd_{70}$-G	1086	1094	[51]
780,000	2-Propanol	356	7	Fe-SBA-15	2065	42	[16]

Average relative atomic mass of alloy was employed to get the concentration of active center.
[a] C_{center} = catalyst dosage (mg)·the fraction of catalytic active center ($\%_{wt}$)·relative atomic $mass^{-1}$.
[b] Calculated by employing equation: Activity = C_{NB}·Conversion·$C_{center}{}^{-1}$·$Time^{-1}$.

10.1 nm:

$$k_{app} = \frac{0.2 \cdot C_{BH_4^-}^{0.6}}{(1 + 6.32 \cdot C_{NB} + 0.14 \cdot C_{BH_4^-}^{0.6})^2} \quad (5)$$

5.6 nm:

$$k_{app} = \frac{0.2 \cdot C_{BH_4^-}^{0.6}}{(1 + 4.38 \cdot C_{NB} + 0.12 \cdot C_{BH_4^-}^{0.6})^2} \quad (6)$$

2.6 nm:

$$k_{app} = \frac{0.007 \cdot C_{NB}^{-0.1} \cdot C_{BH_4^-}^{1.3}}{(1 + 0.73 \cdot C_{NB}^{0.9} + 0.0025 \cdot C_{BH_4^-}^{1.3})^2} \quad (7)$$

Fig. 8 displays the 3D plots of k_{app} as a function of C_{NB} and $C_{BH_4^-}$ obtained from the L-H model (Eqs. (5)–(7)), and the experimental and calculated values of k_{app}. Despite of Pd nanocrystal size, the deviations between the experimental and calculated values are all less than 10%, indicating that the obtained experimental kinetics values can be fully described by the L-H model.

Table 2 compares the activities of our pseudohomogeneous catalyst and some reported heterogeneous catalysts for reduction of NB. In this case, the activity is defined as the number of moles of reduced NB per mole of active components per hour for better comparison of different reaction systems. By comparison, it can be obviously found that the catalytic activity of 2.6 nm Pd nanocrystals was 8009 mol NB h^{-1} (mol Pd)$^{-1}$, which is several or even hundreds of times than other catalysts [15,16,45–51]. Such an excellent catalytic performance should be attributed to high stability and dispersity of Pd nanocrystals in aqueous medium. This will be very beneficial to a complete contact between the reactant and the catalyst with scarcely any diffusion resistance.

In this study, DFT calculations were also employed to better understand the catalytic reduction of NB over monodisperse Pd nanocrystals at the atomic and molecular levels. Various types of reaction sites (including steps and edges) are independent of the nanocrystal shape due to the coordination environment [19]. In this case, terrace sites are major reaction sites. Herein, Pd(1 1 1) and Pd(2 0 0) surfaces, which are the thermodynamically most stable facet, were used to represent the terrace sites of Pd nanoparticles. Fig. 9 depicts the optimized configurations of absorbed nitrobenzene on the Pd(1 1 1) and Pd (2 0 0) surfaces. The corresponding bond lengths of N-O, Pd-H, Pd-O and adsorption energies are listed in Table 3. It should be emphasized that both the phenyl- and nitro-groups are likely to bind to Pd surface free sites, so the research on the adsorption via the phenyl- and nitro-

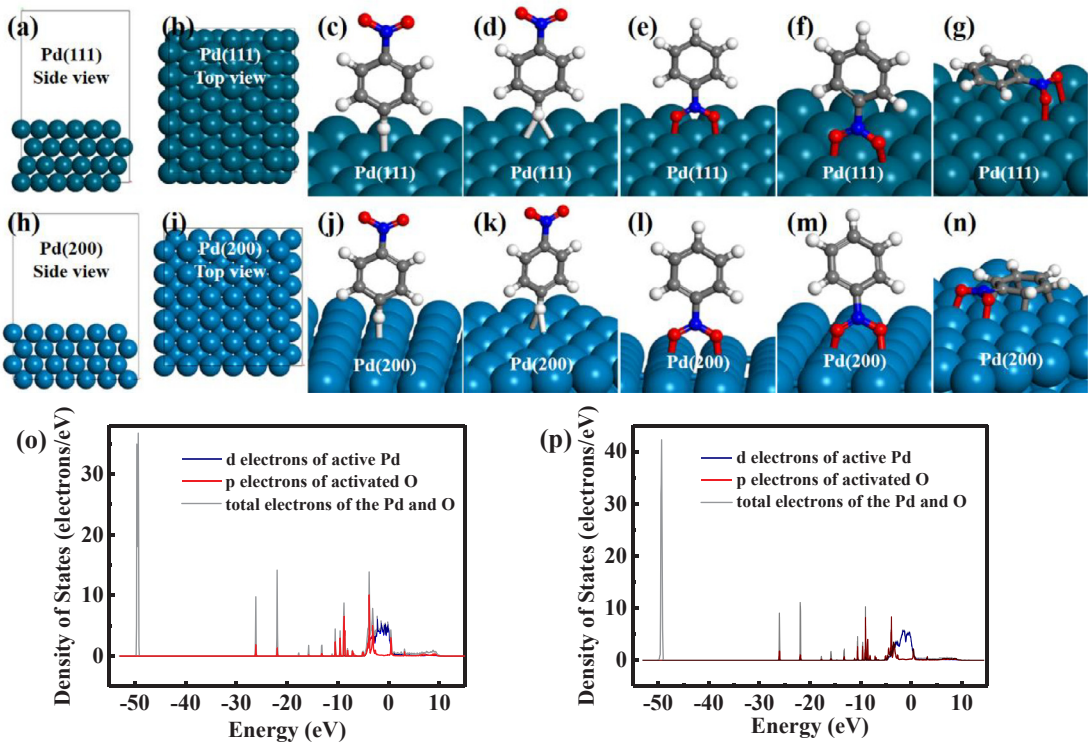

Fig. 9. Pd(1 1 1) surface from the (a) side view and (b) top view. (c–g) Adsorption conditions of NB on Pd(1 1 1) surface. Pd(2 0 0) surface from the (h) side view and (i) top view. (j–n) Adsorption conditions of NB on Pd(2 0 0) surface. (o,p) Density of states (DOS) of Pd and O.

Table 3
Bond lengths (Å) of N-O, Pd-H, Pd-O and corresponding adsorption energy.

Type	c	d	e	f	g	j	k	l	m	n
N-O	1.252/1.252	1.252/1.252	1.269/1.268	1.275/1.265	1.266/1.256	1.251/1.251	1.252/1.251	1.278/1.278	1.280/1.287	1.303/1.303
Pd-H	2.567	2.858/2.951	—	—	—	2.524	2.804/2.941	—	—	—
Pd-O	—	—	2.410/2.432	2.378/2.543	2.690/3.166	—	—	2.275/2.268	2.290/2.276	2.299/2.297
E_{ads}	−0.3091	−0.3069	−0.5338	−0.5331	−0.7737	−0.3003	−0.3080	−0.6917	−0.7242	−1.3176

groups is crucial [52]. When phenyl group is located at the Pd top site (c and j) or bridge site (d and k), the bond length of N-O does not change and remained 1.25 Å. In contrast, if the nitro-group adsorbs at the two neighboring Pd sites via the two O ends (e, g, l and n), the N-O bonds will get active, and adsorption energies will become larger. Furthermore, the paralleled adsorption energies are much larger than vertical adsorptions. Considering the steric hindrance from capping agent, we adjusted the type (e) and (l) to suit for the realistic conditions and got the adsorption type (f) and (m), respectively. Fig. 9(o) and (p) display the density of states (DOS) of adsorption type (f) and (m), respectively. The results indicate the occurrence of the adsorption of active atoms owing to the overlap of the energy levels between Pd 4d and O 2p orbitals.

4. Conclusions

In summary, the highly stable aqueous nanodispersions of monodispersed Pd nanocrystals with tunable sizes of 2.6–10.1 nm are successfully synthesized in a high-gravity RPB reactor. The product in the RPB reactor has a more uniform particle size than that in a stirred tank reactor (STR). And the reaction time is greatly decreased from 3 min (STR) to 1 s (RPB), thereby achieving a continuous preparation. The as-prepared Pd nanocrystals are firstly adopted as a pseudohomogeneous catalyst for the catalytic reduction of NB in aqueous solution and exhibit excellent performance. Ultra-small 2.6 nm Pd nanocrystals have a reaction rate five times as fast as 10.1 nm counterpart. The catalytic reduction of NB and its dependence on the concentrations of reactants can be well described in the Langmuir-Hinshelwood model, with an error ratio below 10%. Density functional theory (DFT) calculations illustrate that NB prefers to adsorb on Pd(2 0 0) surface with the higher adsorption energy. It could be envisioned that this high-gravity route may be an effective and promising strategy for the preparation of monodisperse nanocrystals in large scale as pseudohomogeneous catalyst for highly efficient catalysis.

Acknowledgments

This work was financially supported by National Natural Science Foundation of China (21622601) and National Key R & D Program of China (2017YFA0206801). We are grateful to the “CHEMCLOUDCOMPUTING” of BUCT for computational support.

References

[1] P. Kovacic, R. Somanathan, Nitroaromatic compounds: environmental toxicity, carcinogenicity, mutagenicity, therapy and mechanism, J. Appl. Toxicol. 34 (2014) 810–824.
[2] R.S. Downing, P.J. Kunkeler, H. Van Bekkum, Catalytic syntheses of aromatic amines, Catal. Today 37 (1997) 121–136.
[3] Z.K. Xiong, H. Zhang, W.C. Zhang, B. Lai, G. Yao, Removal of nitrophenols and their derivatives by chemical redox: a review, Chem. Eng. J. 359 (2019) 13–31.
[4] T. Aditya, A. Pal, T. Pal, Nitroarene reduction: a trusted model reaction to test nanoparticle catalysts, Chem. Commun. 51 (2015) 9410–9431.
[5] J.J. Song, Z.F. Huang, L. Pan, K. Li, X.W. Zhang, L. Wang, J.J. Zou, Review on

selective hydrogenation of nitroarene by catalytic, photocatalytic and electrocatalytic reactions, Appl. Catal. B-Environ. 227 (2018) 386–408.
[6] H.K. Kadam, S.G. Tilve, Advancement in methodologies for reduction of nitroarenes, RSC Adv. 5 (2015) 83391–83407.
[7] A.V. Fedorov, A.L. Mikhaylov, A.V. Men"Shikh, D.V. Nazarov, S.A. Finyushin, V.A. Davydov, On the stability of the detonation wave front in the high explosive liquid mixture tetranitromethane/nitrobenzene, J. Energy Mater. 28 (2010) 205–215.
[8] A. Gringauz, Introduction to Medicinal Chemistry: How Drugs Act and Why, Wiley-VCH, 1997.
[9] G.L. Li, W.D. Yin, G.Z. Liu, L.F. Ma, L.Y. Wang, Syntheses structures and magnetic properties of four coordination polymers based on nitrobenzene dicarboxylate and various N-donor coligands, J. Solid State Chem. 220 (2014) 1–8.
[10] K.V.R. Chary, C.S. Srikanth, Selective hydrogenation of nitrobenzene to aniline over Ru/SBA-15 catalysts, Catal. Lett. 128 (2009) 164–170.
[11] C.H. Li, Z.X. Yu, K.F. Yao, S.f. Ji, J. Liang, Nitrobenzene hydrogenation with carbon nanotube-supported platinum catalyst under mild conditions, J. Mol. Catal. A: Chem. 226 (2005) 101–105.
[12] A. Corma, P. Concepción, P. Serna, A different reaction pathway for the reduction of aromatic nitro compounds on gold catalysts, Angew. Chem. Int. Ed. 46 (2007) 7266–7269.
[13] C. Kästner, A.F. Thünemann, Catalytic reduction of 4-nitrophenol using silver nanoparticles with adjustable activity, Langmuir 32 (2016) 7383–7391.
[14] R.F. Nie, J.H. Wang, L. Wang, Y. Qin, P. Chen, Z.Y. Hou, Platinum supported on reduced graphene oxide as a catalyst for hydrogenation of nitroarenes, Carbon 50 (2012) 586–596.
[15] M.M. Dell'Anna, S. Intini, G. Romanazzi, A. Rizzuti, C. Leonelli, F. Piccinni, P. Mastrorilli, Polymer supported palladium nanocrystals as efficient and recyclable catalyst for the reduction of nitroarenes to anilines under mild conditions in water, J. Mol. Catal. A: Chem. 395 (2014) 307–314.
[16] N.S. Sanjini, S. Velmathi, Iron impregnated SBA-15, a mild and efficient catalyst for the catalytic hydride transfer reduction of aromatic nitro compounds, RSC Adv. 4 (2014) 15381–15388.
[17] S. Wunder, Y. Lu, M. Albrecht, M. Ballauff, Catalytic activity of faceted gold nanoparticles studied by a model reaction: evidence for substrate-induced surface restructuring, ACS Catal. 1 (2011) 908–916.
[18] M. Nasrollahzadeh, S.M. Sajadi, A. Rostami-Vartooni, M. Alizadeh, M. Bagherzadeh, Green synthesis of the Pd nanoparticles supported on reduced graphene oxide using barberry fruit extract and its application as a recyclable and heterogeneous catalyst for the reduction of nitroarenes, J. Colloid Interface Sci. 466 (2016) 360–368.
[19] J.H. Lyu, J.G. Wang, C.S. Lu, L. Ma, Q.F. Zhang, X.B. He, X.N. Li, Size-dependent halogenated nitrobenzene hydrogenation selectivity of Pd nanoparticles, J. Phys. Chem. C 118 (2014) 2594–2601.
[20] N. Mei, B. Liu, Pd nanoparticles supported on Fe_3O_4@C: an effective heterogeneous catalyst for the transfer hydrogenation of nitro compounds into amines, Int. J. Hydrogen Energy 41 (2016) 17960–17966.
[21] C.X. Xiao, N. Yan, Y. Kou, Quasi-homogeneous catalysis: towards green and efficiency, Chinese J. Catal. 30 (2009) 753–764.
[22] Z.W. Yan, Y.E. Liu, F.Y. Ma, P. Ge, Preparation of pseudohomogeneous catalyst and its application in coal direct liquefaction, Mod. Chem. Ind. 35 (2015) 119–122 and 124.
[23] M. Biswas, A. Saha, M. Dule, T.K. Mandal, Polymer-assisted chain-like organization of CuNi alloy nanoparticles: solvent-adoptable pseudohomogeneous catalysts for Alkyne-Azide click reactions with magnetic recyclability, J. Phys. Chem. C 118 (2014) 22156–22165.
[24] D. Wenzel, A. Górak, Review and analysis of micromixing in rotating packed beds, Chem. Eng. J. 345 (2018) 492–506.
[25] B.C. Sun, X.M. Wang, J.M. Chen, G.W. Chu, J.F. Chen, L. Shao, Synthesis of nano-$CaCO_3$ by simultaneous absorption of CO_2 and NH_3 into $CaCl_2$ solution in a rotating packed bed, Chem. Eng. J. 168 (2011) 731–736.
[26] C.L. Wei, Z.C. Di, D.H. Zhang, Z.G. Liu, S.H. Li, J.C. Piao, H.L. Wang, Synthesis of modified CeO_2 nanoparticles highly stabilized in organic solvent using higee technology, Chem. Eng. J. 304 (2016) 573–578.
[27] X.J. Huang, X.F. Zeng, J.X. Wang, J.F. Chen, Transparent dispersions of monodispersed ZnO nanoparticles with ultrahigh content and stability for polymer nanocomposite film with excellent optical properties, Ind. Eng. Chem. Res. 57 (2018) 4253–4260.
[28] X.W. Han, X.F. Zeng, J. Zhang, H.F. Huan, J.X. Wang, N.R. Foster, J.F. Chen, Synthesis of transparent dispersion of monodispersed silver nanoparticles with excellent conductive performance using high-gravity technology, Chem. Eng. J. 296 (2016) 182–190.
[29] D.L. Yang, J. Xiao, D. Wang, W.M. Lin, Y. Pu, X.F. Zeng, Y. Le, J.X. Wang, Controllable preparation of monodisperse silica nanoparticles using internal circulation rotating packed bed for dental restorative composite resin, Ind. Eng. Chem. Res. 57 (2018) 12809–12815.
[30] G. Kresse, J. Furthmüller, Efficient iterative schemes for ab initio total-energy calculations using a plane-wave basis set, Phys. Rev. B 54 (1996) 11169.
[31] J.P. Perdew, K. Burke, M. Ernzerhof, Generalized gradient approximation made simple, Phys. Rev. Lett. 77 (1996) 3865.
[32] Y.K. Zhang, W.T. Yang, Comment on "Generalized gradient approximation made simple", Phys. Rev. Lett. 80 (1998) 890.
[33] D. Vanderbilt, Optimally smooth norm-conserving pseudopotentials, Phys. Rev. B 32 (1985) 8412–8415.
[34] M. Dion, H. Rydberg, E. Schroder, D.C. Langreth, B.I. Lundqvist, van der Waals density functional for general geometries, Phys. Rev. Lett. 92 (2004) 246401.
[35] H.Y. Tien, M. Tanniru, C.Y. Wu, F. Ebrahimi, Effect of hydride nucleation rate on the hydrogen capacity of Mg, Int. J. Hydrogen Energy 34 (2009) 6343–6349.
[36] M.H. Entezari, N. Ghows, Micro-emulsion under ultrasound facilitates the fast synthesis of quantum dots of CdS at low temperature, Ultrason. Sonochem. 18 (2011) 127–134.
[37] P. Löbl, M. Huppertz, D. Mergel, Nucleation and growth in TiO_2 films prepared by sputtering and evaporation, Thin Solid Films 251 (1994) 72–79.
[38] Y.W. Tan, X.H. Dai, Y.F. Li, D.B. Zhu, Preparation of gold, platinum, palladium and silver nanoparticles by the reduction of their salts with a weak reductant–potassium bitartrate, J. Mater. Chem. 13 (2003) 1069–1075.
[39] D.V. Leff, P.C. Ohara, J.R. Heath, W.M. Gelbart, Thermodynamic control of gold nanocrystal size: experiment and theory, J. Phys. Chem. 99 (1995) 7036–7041.
[40] T. Teranishi, M. Miyake, Size control of palladium nanoparticles and their crystal structures, Chem. Mater. 10 (1998) 594–600.
[41] M.E. Grass, Y.W. Zhang, D.R. Butcher, J.Y. Park, Y.M. Li, H.D. Bluhm, K.M. Bratlie, T.F. Zhang, G.A. Somorjai, A reactive oxide overlayer on rhodium nanoparticles during CO oxidation and its size dependence studied by in situ ambient-pressure X-ray photoelectron spectroscopy, Angew. Chem. Int. Ed. 47 (2008) 8893–8896.
[42] C. Kastner, A.F. Thunemann, Catalytic reduction of 4-nitrophenol using silver nanoparticles with adjustable activity, Langmuir 32 (2016) 7383–7391.
[43] S. Gu, S. Wunder, Y. Lu, M. Ballauff, Kinetic analysis of catalytic reduction of 4-nitrophenol by metallic nanoparticles immobilized in C, J. Phys. Chem. C 114 (2010) 8814–8820.
[44] Z.Y. Wang, Y. Pu, D. Wang, J. Shi, J.X. Wang, J.F. Chen, 3D foam structured nitrogen doped graphene Ni catalyst for highly efficient nitrobenzene reduction, AlChE J. 64 (2018) 1330–1338.
[45] S.I. El, S.M. El Hout, H.M.A. Sheikh, F.A. Hassan, I.A. Harraz, E.A. El Ibrahim Sharkawy, A green chemical route for synthesis of graphene supported palladium nanoparticles: a highly active and recyclable catalyst for reduction of nitrobenzene, Appl. Catal. A: Gen. 503 (2015) 176–185.
[46] Y.M. Lu, H.Z. Zhu, W.G. Li, B. Hu, S.H. Yu, Size-controllable palladium nanoparticles immobilized on carbon nanospheres for nitroaromatic hydrogenation, J. Mater. Chem. A 1 (2013) 3783–3788.
[47] C.K.P. Neeli, P. Puthiaraj, Y.R. Lee, Y.M. Chung, S.H. Baeck, W.S. Ahn, Transfer hydrogenation of nitrobenzene to aniline in water using Pd nanoparticles immobilized on amine-functionalized UiO-66, Catal. Today 303 (2018) 227–234.
[48] O. Metin, H. Can, K. Sendil, M.S. Gultekin, Monodisperse Ag/Pd core/shell nanoparticles assembled on reduced graphene oxide as highly efficient catalysts for the transfer hydrogenation of nitroarenes, J. Colloid Interface Sci. 498 (2017) 378–386.
[49] G. Romanazzi, A.M. Fiore, M. Mali, A. Rizzuti, C. Leonelli, A. Nacci, P. Mastrorilli, M.M. Dell'Anna, Polymer supported nickel nanoparticles as recyclable catalyst for the reduction of nitroarenes to anilines in aqueous medium, Mol. Catal. 446 (2018) 31–38.
[50] Ö. Metin, A. Mendoza-Garcia, D. Dalmızrak, M.S. Gültekin, S. Sun, FePd alloy nanoparticles assembled on reduced graphene oxide as a catalyst for selective transfer hydrogenation of nitroarenes to anilines using ammonia borane as a hydrogen source, Catal. Sci. Technol. 6 (2016) 6137–6143.
[51] H. Göksu, S.F. Ho, Ö. Metin, K. Korkmaz, A. Mendoza Garcia, M.S. Gültekin, S. Sun, Tandem dehydrogenation of ammonia borane and hydrogenation of nitro/nitrile compounds catalyzed by graphene-supported NiPd alloy nanoparticles, ACS Catal. 4 (2014) 1777–1782.
[52] T. Sheng, Y.J. Qi, X. Lin, P. Hu, S.G. Sun, W.F. Lin, Insights into the mechanism of nitrobenzene reduction to aniline over Pt catalyst and the significance of the adsorption of phenyl group on kinetics, Chem. Eng. J. 293 (2016) 337–344.